A fundamental mode, high-power, large-orbit gyrotron using a rectangular interaction region

D. J. Radack, K. Ramaswamy, W. W. Destler, and J. Rodgers
Laboratory for Plasma Research, University of Maryland, College Park, Maryland 20742

(Received 23 October 1991; accepted for publication 22 February 1993)

This paper reports on experimental and theoretical studies of a fundamental mode, large-orbit gyrotron oscillator designed to produce high-power radiation in the rectangular TE_{10} mode at about 650 MHz. A basic linear theory for design and operation is presented and experiments confirm its applicability. Results of initial experiments have demonstrated 40 ± 4.2 MW of microwave radiation in pulses equivalent in duration to the electron beam, corresponding to an efficiency of about 16%. In some cases, much greater power levels of 100 ± 20 MW were observed at the expected frequency but in pulses of very short duration. In both cases, the observed frequency and mode pattern were consistent with operation in the fundamental mode. Experiments also demonstrated that the observed radiation was linearly polarized, as expected.

I. INTRODUCTION

The usual configuration of the interaction region of a gyrotron is a cylindrical, axially symmetric cavity. Electron beams used to drive the instability are usually annular and exhibit either small-orbit or large-orbit (axis-encircling) rotations. Replacing the conventional cylindrical cavity with a structure of rectangular cross section yields a gyrotron that is straightforward to design and has several potential advantages. However, this configuration has received comparatively little experimental attention.

Cylindrical large-orbit gyrotrons have generated high-power electromagnetic radiation in several source configurations (see Ref. 1, and references cited therein). The large-orbit gyrotron has typically been used to generate high-power radiation at relatively high frequencies due to the potential for efficient beam-wave coupling at high harmonics of the electron cyclotron frequency, ameliorating the requirements of high magnetic fields for gyro-based sources. However, a large-orbit gyrotron is also an attractive low-frequency radiation source, where it offers several advantages over other candidates such as the magnetron, the backward-wave oscillator (BWO), and conventional (small-orbit) gyrotrons.

The peak power capability of the magnetron and BWO is, in many cases, limited by the presence of the periodic, slow-wave structure. In addition, these sources require mechanical changes of the slow-wave circuit to alter the resonant frequency, unlike a gyrotron. The conventional gyrotron is a fast-wave device, but typically uses a magnetron injection gun (MIG) with a thermionic cathode to produce an electron beam with the small velocity spread and other parameters necessary for stable, efficient operation. Frequency scaling of a conventional MIG is a fundamental constraint that does not favor decreasing interaction frequency.[2] In addition, there are practical limitations on the maximum MIG voltage due to breakdown across the insulators. On the other hand, the large-orbit gyrotron may be driven by an electron beam generated via a more Pierce-like diode geometry. Typically for a low-frequency gyrotron, such a diode geometry has advantages over that of a MIG. For example, the current of a cusp-injected large-orbit beam can be greater than that of a MIG[2,3] while the beam width is smaller and the overall beam size is approximately half that from the MIG. Also, for a given frequency of radiation, use of the cusp-injected large-orbit beam configuration avoids many of the problems associated with space-charge effects in the MIG and adjacent compression regions, which can prevent the beam from attaining a large perpendicular velocity or lead to an unacceptably large spread in beam energy.

Analogous large-orbit gyrotron experiments have been conducted in the cylindrical geometry, generating fundamental TE_{11} mode radiation at high-power levels of about 100 MW, corresponding to a peak electronic efficiency of about 18%.[4,5] There are several potential applications where it may be desirable to generate linearly polarized TE_{10} radiation directly, rather than attempting to convert from cylindrical TE_{11} to rectangular TE_{10} through use of a mode converter. Although converters may be designed to perform rather efficiently, these components invariably have insertion losses, can cause spurious mode conversion to unwanted modes, and can adversely affect the operation of the gyrotron by altering the Q of the interaction region.[6] In addition, at frequencies below 1 GHz, the lengths required for low-VSWR transitions may be impractically long, precluding development of a compact source. Furthermore, in the amplifier case, the design of an input coupler may be simplified in the rectangular geometry. Finally, if properly designed, the coupling between the beam and electromagnetic field in the rectangular interaction region may exceed that of a cylindrical interaction region.

In this paper, we report the theoretical design and first experimental operation of a rectangular large-orbit gyrotron operating at the fundamental of the cyclotron frequency (about 650 MHz). High-power radiation in the desired TE_{10} rectangular mode has been observed at frequencies consistent with predictions from linear theory. Basic design, growth rate, and power calculations are presented in Sec. II of this paper. Experimental results are discussed in Sec. III, and conclusions drawn in Sec. IV.

 0021-8979/93/128139-07$06.00

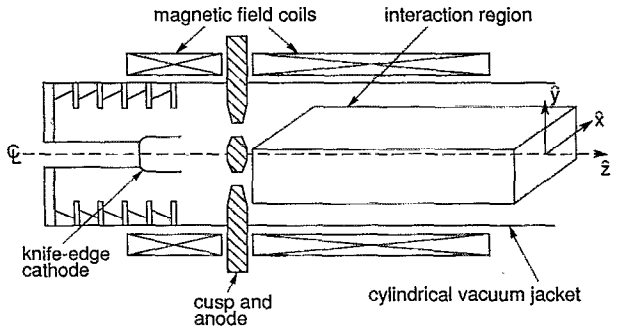

FIG. 1. Cross-sectional view of the fundamental mode large-orbit gyrotron using a rectangular interaction region. The rectangular interaction region is shown obliquely for clarity.

TABLE I. Design parameters of the rectangular large-orbit Gyrotron experiment.

Design parameters	
a	27 cm
b	16.3 cm
Interaction length	127 cm
Beam radius	7.65 cm
Magnetic field (balanced cusp) B_0	0.0380 T
Beam current	600 A–1 kA
V	600 kV
Radiation frequency	~650 MHz
Normalized growth rate	0.145
α	~2

II. THEORETICAL DEVELOPMENT

Operation of the rectangular large-orbit gyrotron is analogous to that of the cylindrical large-orbit gyrotron.[4] A schematic cross section of the rectangular large-orbit gyrotron is shown in Fig. 1. A streaming annular beam passes through a narrow region where the axial magnetic guide field undergoes an abrupt reversal in polarity, a cusp. Downstream of the cusp, the beam rotates as it enters the smooth-walled interaction region. While initially random in phase, the rotating beam is subject to the negative mass instability, promoting the formation of bunching in the electron beam. The entire process is greatly enhanced when a background electromagnetic field is present and synchronism between the electron beam and the electromagnetic field is established.

Linear theory sufficiently describes the behavior of the rectangular gyrotron for first-order tube design purposes. Other numerical and nonlinear techniques have been developed to model gyro-based devices, and may be more appropriate for accurately modeling the performance of the rectangular gyrotron oscillator. However, the linear theory is attractive in this case because it yields closed-form analytic expressions that illuminate the physics and scaling laws governing source behavior.

Consider a tenuous annular electron beam, $\delta(r-r_b)$, monoenergetic and possessing only axial ($v_{z0}=\beta_{z0}c\hat{z}$) and azimuthal ($v_{\theta 0}=\beta_{\theta 0}c\hat{\theta}$) velocities, and propagating through a rectangular interaction region immersed in a uniform axial magnetic field, $B_0\hat{z}$. In the absence of any perturbations caused by the presence of the electron beam, the dispersion relation relating to waveguide modes is

$$\omega^2=(k_z c)^2-\omega_{co}^2, \tag{1}$$

where k_z is the axial component of the wave vector and $\omega_{co}^2=\pi^2c^2[(m/a)^2+(n/b)^2]$ is the cut-off frequency for the mode of interest. Doppler-shifted cyclotron harmonics are associated with beam density perturbations caused by rotation and are given by

$$\omega=k_z v_z+l\Omega_c, \tag{2}$$

where v_z is the axial velocity of the beam, l is the harmonic number, $\Omega_c=qB_0/\gamma m_0$, γ is the relativistic factor, and m_0 is the electron rest mass. Simultaneous solution of Eqs. (1) and (2) yields the points where synchronism occurs and growth rates are greatest. In general, two solutions result. However, for the grazing condition, the two converge to a single operating point, given by the expression

$$k_z c=\gamma_z^2 l\Omega_c\beta_{z0}, \tag{3}$$

where $\gamma_{z0}^{-2}=1-\beta_{z0}^2$, l is the beam cyclotron harmonic number, and $\Omega_c=qB_0/\gamma_0 m_0$ is the relativistic cyclotron frequency. For the grazing condition, it is necessary that experimental parameters be chosen such that

$$\omega_{co}=\gamma_{z0}l\Omega_c. \tag{4}$$

The electron beam radius necessary for synchronism ($l=1$ fundamental assumed) is found from the inequality

$$\frac{\sqrt{mb+na}}{ab}r_b=\frac{1}{\pi}\frac{\chi}{\sqrt{1+\chi^2}}, \tag{5}$$

where $\chi=\alpha\sqrt{\gamma_0^2-1}$ and $\alpha=v_\perp/v_z$. Here, the electromagnetic field is either TE_{mn} or TM_{mn} and the waveguide is rectangular with inner dimensions a and b. Assuming resonance with the fundamental mode, a large fraction of rotational energy, and a fairly relativistic beam energy, Eq. (5) may be approximated by $r_b\approx a\sqrt{b}/\pi$. Typical design parameters are summarized in Table I and the dispersion relation is plotted in Fig. 2.

Several techniques are available to analyze the beam-wave coupling in this system. Lau and Barnett proposed an analytic model based on several simplifying assumptions to determine the coupling parameter and growth rate of the fundamental TE mode in the rectangular interaction region.[7] Later, Ferendeci and Han rigorously solved the linearized relativistic Vlasov equation, obtaining general solutions for TE_{mn} modes.[8] These techniques are often most appropriate in the small-signal regime. To model the large-signal behavior of the source, other approaches including numerical integration of the nonlinear ballistic equations have been developed for analysis of the conventional gyrotron.[9] In principle, these techniques could be employed to design and analyze the rectangular gyrotron with some modification due to the lack of cylindrical symmetry. As the nature of these experiments were proof-of-principle, the approach using the linearized Vlasov equation was followed.

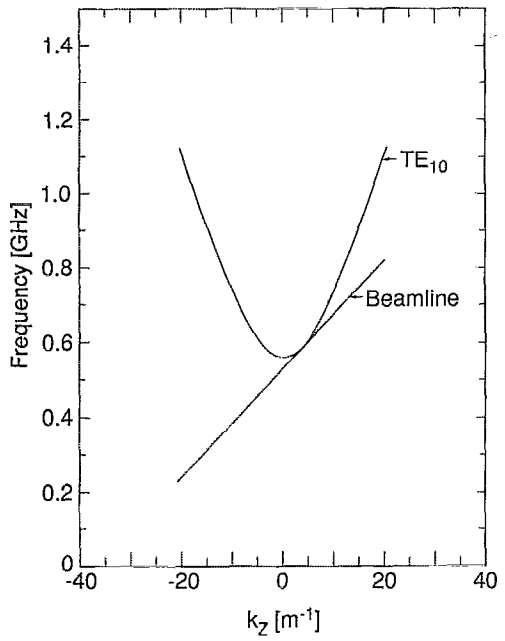

FIG. 2. Dispersion relation for the design parameters in Table I and used in the experiments.

In Lau and Barnett's model, the electron beam is assumed to be infinitely thin, monoenergetic, guiding center radius of zero, and $v_z=0$. Under these assumptions, self-fields are neglected, the electrons have no velocity spread in either the transverse or axial direction, and no radial velocity component. Since, to lowest order, the coupling and growth rate are independent of v_z and k_z, the $v_z=0$ assumption only serves to simplify the calculation.[7] The coupling term is determined by calculating the rf surface current induced on the beam, then using that result in the wave equation for TE modes. The coupling term ϵ for the TE_{10} rectangular mode to a rotating electron beam of radius r_b is given by

$$\epsilon_{TE_{10}}=\frac{8\nu}{\pi\gamma_0}\frac{a}{b}(\alpha\beta_z)^2\left[J_l'\left(\frac{\pi r_b}{a}\right)\right]^2, \tag{6}$$

where ν is the dimensionless Budker parameter and J_l' is the derivative with respect to the argument of the Bessel function of the first kind, of order one. Note that the coupling scales linearly with the ratio of the waveguide dimensions. Furthermore, Lau showed that when $a/b>2$, the growth rate of the fundamental rectangular mode exceeds that associated with an analogous fundamental cylindrical mode. From the coupling coefficient the TE_{10} growth rate Γ may be calculated from the expression

$$\Gamma_{TE_{10}}=\frac{\sqrt{3}}{2}\left[\frac{\epsilon_{TE_{10}}}{2}\right]^{1/3}. \tag{7}$$

The rigorous, more generalized solution for the dispersion relation of the rectangular gyrotron yields a result that is mathematically similar to that of an axis-symmetric system with one significant difference. The dispersion of a given mode in the rectangular case is determined by an infinite summation of harmonic terms, rather than a single quantity. Solving the dispersion relation in the usual manner for the coupling terms yields a result mathematically similar to Eq. (6), with one significant addition. The right-hand side is multiplied by the beam-wave coupling coefficient

$$F_l(k_{xm},k_{yn},x_0,y_0)$$
$$=\tfrac{1}{2}((-1)^l\{e^{jk_{xm}x_0}\cos[k_{yn}y_0+l\tan^{-1}(k_{yn}/k_{xn})]\}$$
$$+\{e^{-jk_{xm}x_0}\cos[k_{yn}y_0-l\tan^{-1}(k_{yn}/k_{xn})]\}), \tag{8}$$

where $(0\leqslant|F_l|\leqslant1)$, k_{xm}, and k_{yn} are the transverse wave vector components, and (x_0,y_0) give the displacement of the beam's coordinate origin from the center of the rectangular waveguide.

As is typically done in the design of gyrotrons, parameters are chosen for a grazing interaction, where the lth harmonic of the beam line is tangential to the mode of interest. The grazing condition is a desirable operating point for the gyrotron because it is both strong and efficient; for a given l, the forward-wave growth rates are maximum and the group velocities of the electron beam and electromagnetic wave are identical, so that energy in the waveguide propogates at the same velocity as the perturbation. A peculiarity occurs in the rectangular gyrotron operating in a TE_{m0} mode since $\omega_{co}\propto m$. Therefore, the larmor radius required for a grazing interaction between the $l=1$ beam mode and the TE_{10} mode is identical to that required for grazing between the $l=m$ beam mode and the TE_{m0} mode. The growth rates for several such cases are shown in Table II. Note that the fundamental interaction dominates. Designing a rectangular interaction region for grazing intersection near cutoff, between the TE_{10} and $l=1$ cyclotron harmonic will always result in the largest growth rate. The beam-wave coupling for grazing in that case, ϵ_{10}^1, will always exceed $\epsilon_{mn}^{l>1}$.[7]

Although the fundamental interaction is expected to dominate, the growth rates of other grazing harmonics may produce some mode competition. In addition, if the electron beam is displaced from the center of the waveguide, there may be significant coupling to other higher order modes. The coupling to TM modes is expected to be weak because the electric field associated with those modes is not oriented to couple well with a rotating electron beam in a rectangular waveguide. Assuming the beam is centered

TABLE II. Coupling coefficients and growth rates for the possible tangential interactions.

TE mode	l	$\epsilon_{mn}^l=a\times10^{-3}$ a	Normalized growth rate $\frac{\Gamma}{\Omega_r}$
TE_{10}	1	9.2	0.145
TE_{20}	2	4.2	0.110
TE_{30}	3	2.5	0.090
TE_{40}	4	1.7	0.080
TE_{50}	5	1.2	0.070

TABLE III. Predicted resonant frequencies in the order of increasing TE mode cut-off frequency.

TE mode	l	ω_-	ω_+	$\omega_{\tan}$
TE_{10}	1	⋯	⋯	~650 MHz
TE_{11}	2	~1.085 GHz	~1.200 GHz	⋯
TE_{20}	2	⋯	⋯	~1.238 GHz
TE_{21}	3	~1.47 GHz	~1.95 GHz	⋯
TE_{30}	3	⋯	⋯	~1.831 GHz

in the waveguide channel, analysis of the coupling equation shows that when the sum of the electromagnetic mode indices $(m+n)$ is odd (even), coupling with odd (even) beam modes dominates over the converse situation. In the converse case, net energy exchange does not readily occur because the rf electric field associated with those modes is not oriented to synchronously promote bunching; the orbit-averaged force experienced by an electron ensemble is zero.

Assuming beam and waveguide parameters from this experiment (see Table I), the predicted resonant frequencies for several salient modes are shown in Table III. In most cases, two resonant frequencies exist, corresponding to the high and low intersection of Eqs. (1) and (2). Note that $\omega_{\tan}$ exists only for tangential interactions, where ω_+ and ω_- coalesce. The real frequency shift due to the presence of the beam was taken into account for the cases where it is not negligible. Note that the dimensions of the interaction region were chosen such that there was a reasonable frequency separation between modes, decreasing undesired coupling, and easing the identification of higher order harmonics. During the experiment, however, it is quite possible that the frequency generated may differ from that predicted by theory for a variety of reasons related to the stability of and uncertainty in the beam and system parameters. For example, the high-voltage pulse that creates the beam is fairly flat, but does have a slight ripple, on the order of a few percent. The beam energy may vary from shot-to-shot due to fluctuations in the capacitor charging voltage or due to the varying condition of the beam diode. Also, the magnetic field has a finite transition length and some inhomogeneities. Besides possibly altering the interaction frequency, the magnetic field transition length and axial profile can adversely affect the rotation of the beam.[10]

Assuming operation in the fundamental mode, an estimate of the total power radiated by an open-ended rectangular source may be determined through the use of the following relation for the on-axis microwave power density measured in the far field:

$$p_{\max}=\frac{(ab)^2}{2\eta(\pi r\lambda)^2}\left(\frac{\eta k_0}{\omega\mu_0}+1\right)^2 E_i^2, \tag{9}$$

where $p_{\max}$ is the power density at the receiving antenna horn, η and μ_0 are the impedance and permittivity of free space, k_0 is the propagation constant in the waveguide, and E_i is the electric field at the end of the radiating waveguide. Solving Eq. (9) for E_i, the total radiated power is easily calculated from

$$P=\frac{1}{2}E_i^2\frac{k_0}{\omega\mu_0}\frac{ab}{2}. \tag{10}$$

III. EXPERIMENTAL RESULTS

A rectangular gyrotron oscillator experiment was designed to generate electromagnetic radiation at 650 MHz radiation in the fundamental rectangular mode, TE_{10}. A cross section of the experimental setup was shown in Fig. 1. The rectangular interaction region was designed for compatibility with the vacuum envelope associated with an existing cylindrical gyrotron, hence the design values from Table I represent the best choices from tradeoffs and are not necessarily representative of an optimized source.

The pulsed power supply used in these experiments was capable of delivering about 600 keV to the high impedance diode.[11] A pulse flat-top of about 75 ns and about 4% ripple was obtained by use of a high-power resistor (sodium-thiosulfate liquid—$Na_2S_2O_3$) to match the parallel combination to the low impedance charge line. The electron beam source consisted of an explosive-emission stainless steel, knife-edge cathode separated by a short gap (~4.5 cm) from a grounded anode plate with an annular aperture. That anode plate was mounted to the upstream-side of a magnetically soft ferromagnetic plate. A set of solenoidal field coils placed upstream and downstream of the iron plate form the magnetic cusp. When the coils are energized, they create a solenoidal guide field in the regions away from the cusp. At the cusp, the ferromagnetic material guides magnetic flux lines, creating an essentially radial magnetic field from the axial guide field. As a streaming electron passes through the cusp, it begins to rotate due to the Lorentz force $v_0\hat{z}\times B\hat{r}$. Depending on the polarity and magnitude of the electric currents in the solenoids, either large- or small-orbit rotations may be imposed on the streaming electron beam.[3] If the electric currents in the upstream and downstream field coils are chosen such that the axial magnetic field on each side are equal and opposite, then the cusp is balanced and electrons within the beam undergo helical orbits, their downstream trajectories encircling the $\hat{z}$ axis. In the balanced cusp case, the guiding center is zero. The period and axial length of a single electron's helical trajectory is determined by the initial beam radius, energy, and strength of the externally applied magnetic field. For a balanced cusp, the α of the beam is given by

$$\alpha=\frac{r_b q B_0}{\sqrt{[(m_0c)^2(\gamma_0^2-1)-(r_b q B_0)^2]}}. \tag{11}$$

Typically, the injected electron beam carried a current between 600 and 900 A, depending on the anode-cathode gap, charging voltage, and magnetic field setting. A threshold energy is associated with the electron beam since, for a given set of magnetic fields, the cusp reflects all electrons with energies below:

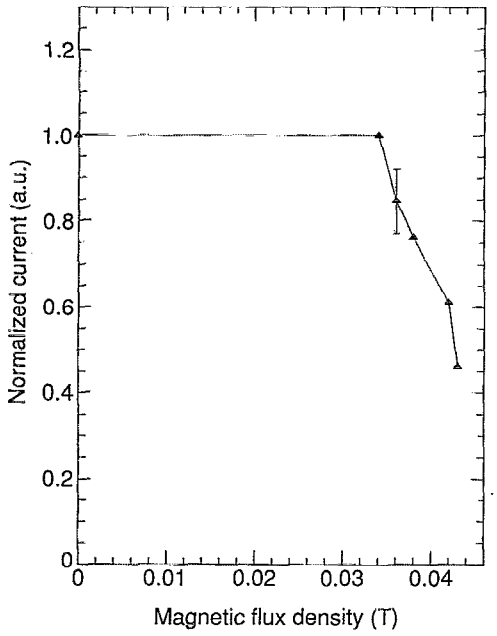

FIG. 3. Graph of the normalized beam current vs the magnetic flux density on either side of the balanced cusp. The current is normalized to 600 A. The anode-cathode gap was about 5 cm for this investigation.

$$\gamma_{\rm th}=\sqrt{\left(\frac{qr_bB}{mc}\right)^2+1}. \tag{12}$$

Figure 3 displays downstream beam current vs applied magnetic field measured using a low inductance Faraday cup. From this data, the beam energy is calculated to be between 500 and 600 keV, the maximum accelerating potential.

All microwave measurements were made using the diagnostic setup shown in Fig. 4. Radiation was extracted through the open-ended waveguide and radiated into free space. An open-ended WR-975 receiving antenna was placed in the far-field, oriented first to couple best to modes with an E_y. Later, the antenna was reoriented by a quarter ccw rotation to couple best with modes that have an E_x. The microwaves received during a shot were coupled to a

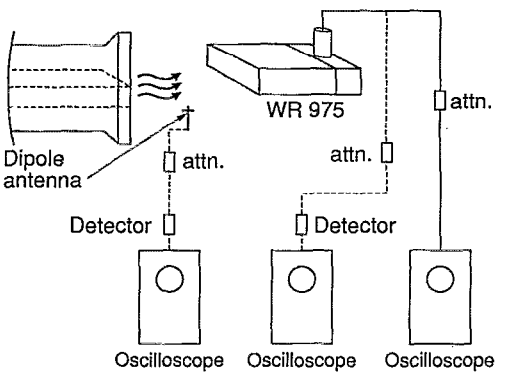

FIG. 4. Diagnostic setup for the investigation of radiation. The receiving horn was located in the far field.

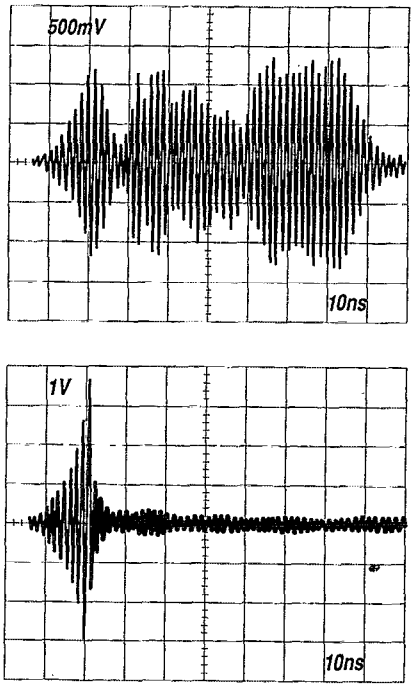

FIG. 5. (a) Typical example of the raw rf waveform during long-pulse operation; (b) typical example of the raw rf waveform during short-pulse operation. The attenuation used on the fast oscilloscope differs between the two bursts.

coaxial line, attenuated, and either observed directly with a fast oscilloscope or detected by a calibrated diode. The effective area of the WR-975 antenna was determined through external calibration. All cables and attenuators were calibrated *in situ* and independently. The connections and transitions were all carefully shielded to minimize leakage. Similar diagnostic techniques have been shown to provide accurate results for measurements of this type and magnitude.[4] In addition, the breakdown of a low-pressure gas cell was used to confirm the lower bound of the radiated power.

For certain parameters, the duration of the microwaves radiated by the rectangular gyrotron were about that of the beam pulse (75 ns), while occasionally, much higher powers (two to three times) were observed, but in very short pulses. Typical examples of observed microwave radiation is shown in Figs. 5(a) and 5(b). Fourier decomposition of the spectral frequency components present in the pulse of Fig. 5(a) is shown in Fig. 6. The observed frequency of radiation, about 650 MHz, is consistent with the predicted result from linear theory. Using Eq. (10), the estimated total power radiated by the source is estimated to be about 40 MW for the long pulse case, typified by Fig. 5(a). Operation at this power level corresponds to an electronic efficiency of about 16%. Powers as high as 120 MW were observed in short pulses, often at high charging voltages and high α, but not consistently. Reducing the charging voltage could usually restore long-pulse operation, while altering the magnetic field was less likely to do so.

The dependence of the radiated power with the cusp magnetic flux density was investigated. The cusp was kept

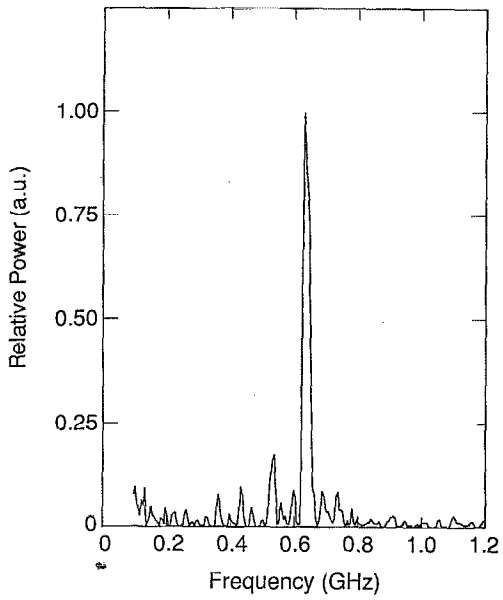

FIG. 6. Fast Fourier transform of the raw waveform from a typical long-pulse shot.

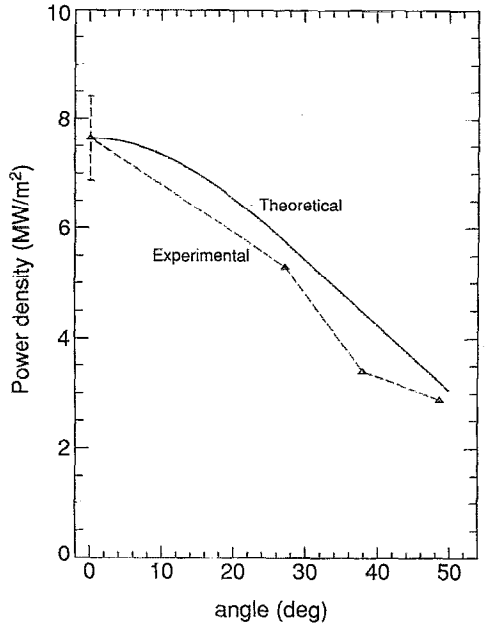

FIG. 8. Radiated power denisty at the receiving antenna vs the angle between the $\hat{z}$ axis and the receiving antenna. All measurements were made on a constant horizontal plane. Note that the experimental power levels are in good agreement with theoretical calculations.

balanced, but varied between 340 and 400 G. For each shot, the beam energy was kept constant. The results are shown in Fig. 7. For this particular case, $qV_b \approx 500$ keV, the power peaked at about 355 G. At lower flux densities, the power level is depressed because the α is small, while at greater magnetic flux densities, the injected beam current decreases due to higher threshold electron energy selection by the cusp.

The radiation pattern from the rectangular gyrotron was determined by surveying the position of the WR-975 antenna at various angles, while keeping the distance between the radiating and receiving antennas constant. Results are shown in Fig. 8. It is clear that the radiated power is maximum on center and is about 3 db down at an angle of 30°. Also plotted is a theoretical curve of the expected far-field TE_{10} radiation pattern. The two are in good agreement. In addition, numerically integrating the power levels received yields a bound on the power that is fairly near 40 MW, as predicted by Eq. (10).

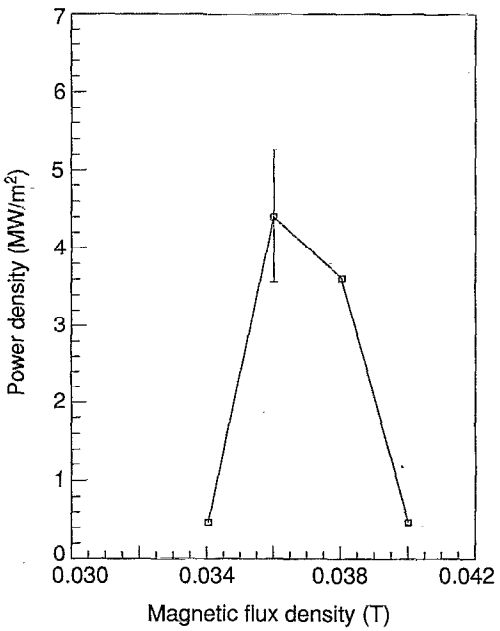

FIG. 7. Radiated power density at the receiving antenna (on axis) vs magnetic flux density adjacent to the balanced cusp.

In other experiments, the orientation of the receiving waveguide was changed by rotation of a quarter turn. The antenna was then situated to couple best to electromagnetic modes that have an E_x. On axis, the measured power levels were approximately 8 dB lower than the previous case, evidence of linear polarization. As the WR-975 horn was surveyed off-axis, a narrow radial band of relatively high-power radiation was observed, peaking at about 45°. The frequency of the radiation was beyond the bandwidth of the fast oscilloscope (BW $\approx$ 1.2 GHz) and was not investigated in great detail. The total power radiated at that harmonic was much smaller than the fundamental.

IV. CONCLUSIONS

A rectangular interaction region was designed for a fundamental-mode large-orbit gyrotron. Operation of the gyrotron as a high-power fundamental mode radiation source was confirmed. Experimentally observed parameters were consistent with the predictions of linear theory. Microwave power of approximately 40 MW was detected in the far field during long pulses, while higher powers ($\sim$100 MW) were also obtained, but were of short duration. The electronic efficiency of the source is estimated to

be about 16% for the long-pulse operation. The radiation was observed at the expected frequency and also found to be linearly polarized. A significant level of power, although considerably less than that in the fundamental, was observed in a harmonic interaction.

As implemented in these experiments, the rectangular interaction region was not optimized for best coupling, but was designed for compatibility with an existing apparatus. Future experiments may address that issue, however. The issues associated with the harmonic interaction will be addressed as well.

ACKNOWLEDGMENTS

The authors are pleased to acknowledge useful discussions with Y. Y. Lau, who first suggested the experiment. Technical assistance from John Pyle and Doug Cohen are greatly appreciated. We are grateful for the loan of the WR-975 waveguide and Tektronix 7104 oscilloscope from the Harry Diamond Laboratory. This research was supported by the AAI Corporation and the Maryland Industrial Partnerships Program.

[1] W. W. Destler, E. Chojnacki, R. F. Hoeberling, W. Lawson, A. Singh, and C. D. Striffler, IEEE Trans. Plasma Sci. **PS-16**, 71 (1988).
[2] W. Lawson, IEEE Trans. Plasma Sci. **PS-16**, 290 (1988).
[3] W. Lawson and P. E. Latham, J. Appl. Phys. **61**, 519 (1987).
[4] W. W. Destler, K. Irwin, W. Lawson, J. Rodgers, Z. Segalov, E. P. Scannell, and S. T. Spang, J. Appl. Phys. **66**, 4089 (1989).
[5] K. Irwin, M. S. thesis, University of Maryland (1990).
[6] L. Ives, K. Felch, C. Hess, H. Jory, R. Pendleton, A. LaRue, M. Chodorow, J. Feinstein, L. Zitelli, and R. Martorana, Int. Electron Devices Meeting, Technical Digest, IEEE Cat. No. 88CH2528-8, pp. 152–154 (1988).
[7] Y. Y. Lau and L. R. Barnett, IEEE Trans. Electron Devices **30**, 908 (1983).
[8] A. M. Ferendeci and C. C. Han, IEEE Trans. Electron Devices **31**, 1212 (1984).
[9] B. Levush, in *High Power Microwave Sources*, edited by V. L. Granatstein and I. Alexeff (Wiley, New York, 1984), p. 127.
[10] M. J. Rhee and W. W. Destler, Phys. Fluids **17**, 1574 (1974).
[11] A. Shpilman, M. S. thesis, University of Maryland (1983).